AD-A083 626 DEL MAR TECHNICAL ASSOCIATES CA F/G 8/11
BODY WAVE INVERSION USING TRAVEL TIME AND AMPLITUDE DATA.(U)
JAN 80 A JURKEVICS, R WIGGINS, L CANALES N00014-78-C-0061
UNCLASSIFIED DELTA-R-79-0030 NL

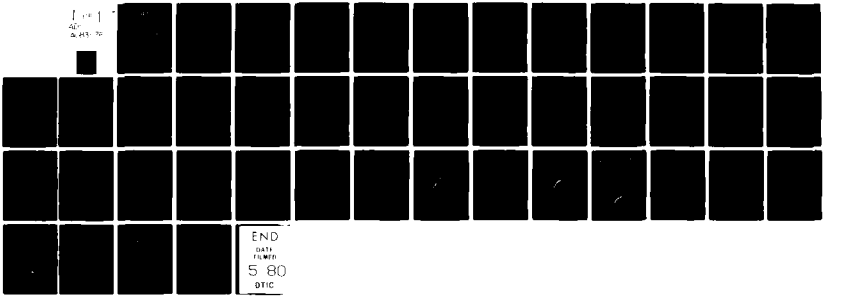

Report DELTA-R-79-0030

LEVEL II

# BODY WAVE INVERSION USING TRAVEL TIME AND AMPLITUDE DATA

Andrejs Jurkevics
Ralphe Wigginst
Luis Canales*

Del Mar Technical Associates
P.O. Box 1083
Del Mar, California 92014

†Now at Mobile R&D Corp.
Dallas, Texas

*CICESE
Ensenada, Baja California, Mexico



23 January 1980

Final Report
Contract No. N0014-78-C-0061

UNLIMITED DISTRIBUTION



Prepared for

OFFICE OF NAVAL RESEARCH
Ocean Acoustics Program
Ocean Science & Technology Division
NSTL Station, MS 39529

UNCLASSIFIED

SECURITY CLASSIFICATION OF THIS PAGE (When Data Entered)

| REPORT DOCUMENTATION PAGE | READ INSTRUCTIONS BEFORE COMPLETING FORM |
|---|---|
| 1. REPORT NUMBER: DELTA-R-79-0030 | 2. GOVT ACCESSION NO.: AD-A093626 | 3. RECIPIENT'S CATALOG NUMBER: |
| 4. TITLE (and Subtitle): Body Wave Inversion Using Travel Time and Amplitude Data | 5. TYPE OF REPORT & PERIOD COVERED: Final Report |
| | 6. PERFORMING ORG. REPORT NUMBER: DELTA-R-79-0030 |
| 7. AUTHOR(s): Andrejs Jurkevics, Ralphe Wiggins, Luis Canales | 8. CONTRACT OR GRANT NUMBER(s): N00014-78-C-0061 |
| 9. PERFORMING ORGANIZATION NAME AND ADDRESS: Del Mar Technical Associates, P. O. Box 1083, Del Mar, California 92014 | 10. PROGRAM ELEMENT, PROJECT, TASK AREA & WORK UNIT NUMBERS: 23 Jan 80 |
| 11. CONTROLLING OFFICE NAME AND ADDRESS: Office of Naval Research, Code 486, 800 North Quincy, Arlington, VA 22217, ATTN: Dr. J. M. McKisic | 12. REPORT DATE: January 23, 1980 |
| | 13. NUMBER OF PAGES: 43 |
| 14. MONITORING AGENCY NAME & ADDRESS (if different from Controlling Office): N/A | 15. SECURITY CLASS. (of this report): Unclassified |
| | 15a. DECLASSIFICATION DOWNGRADING SCHEDULE: N/A |

16. DISTRIBUTION STATEMENT (of this Report)

Unlimited

17. DISTRIBUTION STATEMENT (of the abstract entered in Block 20, if different from Report)

N/A

18. SUPPLEMENTARY NOTES

Accepted for publication in Geophysical Journal of the Royal Astronomical Society

19. KEY WORDS (Continue on reverse side if necessary and identify by block number)

Body Waves
Seismic
Inversion of Data
Earth Structure
Non-uniqueness
$L_1$ norm
Disc Ray Theory

20. ABSTRACT (Continue on reverse side if necessary and identify by block number)

An interpretation scheme has been developed for the determination of laterally homogeneous earth structure using body-wave travel time and amplitude data. A family of p(x) (ray parameter vs distance) functions consistent with the data are obtained as solutions to an inverse problem. Each p(x) solution has a corresponding velocity-depth function which maximizes or minimizes the depth for one velocity. The family of allowable p(x) curves therefore defines a velocity-depth envelope which bounds the range of earth structures consistent with these data.

DD FORM 1 JAN 73 1473 EDITION OF 1 NOV 65 IS OBSOLETE

UNCLASSIFIED 109

SECURITY CLASSIFICATION OF THIS PAGE (When Data Entered)

SUMMARY

An interpretation technique has been developed for the determination of laterally homogeneous earth structure using body-wave travel time and amplitude data. A family of $p(x)$ (ray parameter vs distance) functions consistent with the data are obtained as solutions to an inverse problem. Each $p(x)$ solution has a corresponding velocity-depth function which maximizes or minimizes the depth for one velocity. The family of allowable $p(x)$ curves therefore defines a velocity-depth envelope which bounds the range of earth structures consistent with these data.

## 1 INTRODUCTION

Earth structure cannot be determined uniquely from a finite set of body-wave observations containing errors. In general, there is a broad range of velocity-depth models which are consistent with a given data set. In recent years, several authors, most notably Bessonova, et al. (1974, 1976), have proposed methods for estimating bounds for the allowable earth structures by inverting travel time data. However, since these techniques neglect amplitude information, the resulting bounds are somewhat less restrictive than may be indicated by the observed data. Mellman (1978) has taken a different approach, whereby velocity-depth models are determined by matching the waveforms of observed and synthetic seismograms. The non-uniqueness of the resulting earth models is estimated from the discrepancy between solutions obtained by using different starting models in the inversion scheme.

In the following communication, we propose a technique for interpreting seismic refraction data which incorporates both amplitude and travel time information. The data are inverted to determine the range of seismic velocity-depth models which are consistent with these observations. The earth models in this investigation are restricted to be laterally uniform, since we allow the velocity to vary only as a function of depth. Furthermore, this investigation is restricted to velocity-depth models which contain no low-velocity zones.

The central idea in this interpretation scheme is the choice of the function $p(x)$ (wave slowness as a function of source-receiver distance) for performing the inversion. There are several advantages for deforming the $p(x)$ curve to fit the data:

(a) The travel time at any distance is a linear integral of the $p(x)$ curve.

(b) The velocity-depth ($v(z)$) model can be obtained by a simple linear Weichert-Herglotz integral of the $p(x)$ curve.

(c) Amplitude information can be recovered from the $p(x)$ curve through a simple Disc Ray Theory integration (Wiggins, 1976).

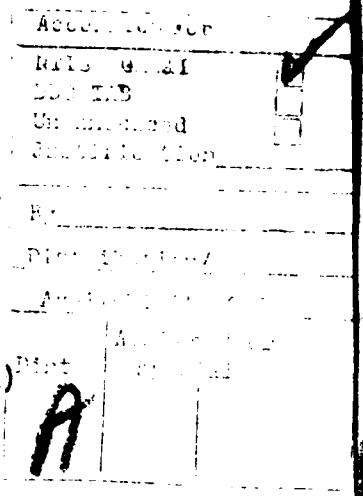

Hence, <u>all</u> of the desired transformations can be made directly from the $p(x)$ curve. These transformations are well-defined and stable functions of the $p(x)$ curve.

Another important reason for choosing the $p(x)$ function for performing the inversion is based on the need for a simple representation of the non-uniqueness. McMechan & Wiggins (1972) and Wiggins, et al. (1973) have shown how the uncertainty of the earth structure can be represented by an envelope in the $p$-$x$ plane, which bounds the set of allowable $p(x)$ curves. They have also shown how the $p(x)$ function can be manipulated in order to determine extremal depths corresponding to any velocity. Their methodology will be used in this interpretation scheme and will, in fact, be incorporated directly into the inverse problem so that extremal depths can be determined for the set of permissable velocity models.

The interpretation procedure involves a combination of forward and inverse modeling. The inverse problem consists of determining the set of $p(x)$ curves for which the velocity-depth functions are extremal. The forward problem consists of determining the synthetic seismograms corresponding to these extremal $p(x)$ solutions. In general, all of the data cannot be fit in one iteration, so the problem proceeds iteratively. The seismograms corresponding to the initial $p(x)$ solutions have amplitudes and travel times which are inconsistent with the observed data. This can be remedied in subsequent iterations by imposing limits which restrict the $p(x)$ curves from certain regions of the $p$-$x$ plane. These bounds form a $p(x)$ envelope which is refined on each iteration until all of the solutions match the observed data to within some uncertainty. The scatter of the calculated seismograms is governed by the width of the

$p(x)$ envelope, which, in turn, determines the range of allowable earth structures.

The interpretation scheme will be illustrated in detail in a later section. First, we turn our attention to the most complex aspect of the procedure — the inverse problem.

## 2 THE INVERSE PROBLEM

The inverse part of the interpretation scheme consists of determining an optimal $p(x)$ curve which satisfies certain travel time constraints and at the same time maximizes or minimizes the depth for some velocity. Both of these conditions are quite straightforward in that they involve transformations from the $T$-$x$ and $v$-$z$ to the $p$-$x$ domains. The transformations are linear and are written mathematically as equalities. However, there are also a number of bounding or inequality constraints which we wish to impose on the $p(x)$ solutions. Two of these require the velocity-depth function corresponding to any $p(x)$ solution to be physically meaningful; that is, the velocity must be single valued in depth and the depths for all velocities must be positive. A third inequality constraint stems from the forward problem, where bounds are imposed on the solutions limiting them from certain regions of the $p$-$x$ plane. Least-squares error techniques are not well suited to problems containing many inequality constraints. We have turned, therefore, to the realm of $L_1$-norm linear estimation in order to solve our inverse problem. However, before we discuss our method for solving it, let's examine the problem more closely.

We cast the inverse problem in the form of a system of equations with the $p(x)$ curve as a vector of unknowns $\bar{x}$, i.e.,

$$\bar{\bar{A}}\,\bar{x} - \bar{d} \simeq \bar{e} \tag{1}$$

where each row has the form

$$\sum_{j=1}^{M} A_{kj}\, x_j - d_k \simeq e_k \,, \qquad k = 1, N \,. \tag{2}$$

Here $\bar{x}$ is the discretized $p(x)$ curve, $\bar{d}$ is the "data" vector, and $\bar{\bar{A}}$ is the transfer matrix which relates the unknowns $\bar{x}$ to the "data" $\bar{d}$. The optimum solution for $\bar{x}$ is determined by minimizing the error vector $\bar{e}$ in some way.

The unknowns in this problem are chosen to be the discrete source-receiver distances $x_j$, $j = 1, M$ corresponding to finite samplings $p_j$, $j = 1, M$ of the ray parameter over some interval of interest $[p_{min}, p_{max}]$. The distance $x$ is chosen to be the dependent variable because it is generally interpreted as being single-valued in $p$. (The converse is not true if there are any triplications in the $p(x)$ curve.) We use linear interpolation between the discrete points $x_j$ and $x_{j+1}$ in order to approximate a continuous $p(x)$ curve. We have found that this piecewise linear representation has significant benefits over a constant interpolation scheme, since discretization effects are reduced. (For simplicity, the equations in this communication are presented as having constant interpolation, i.e., as simple summations.)

The $p$ interval depends on the problem at hand and must be determined first. In general, $p_{max}$ is equal to $(\text{velocity})^{-1}$ at the surface and is assumed to be known. The lower limit $p_{min}$ is estimated from the travel time data at large source-receiver distances.

## 3 SOLVING THE INVERSE PROBLEM

The bounding constraints which we impose on the solution manifest as inequality equations. For example, the equations restricting the $p(x)$ curve to lie within some limits $x^{LO}$ and $x^{HI}$ are simply

$$x_j^{LO} \leq x_j \leq x_j^{HI} , \qquad j = 1, M . \tag{3}$$

One way to ensure that such bounding constraints are always satisfied is to insert the relevant equations directly into the inverse problem. Claerbout & Muir (1973) have devised an algorithm for solving an overdetermined system of equations that can be used to include inequality constraints into the problem. Their algorithm optimizes the solution according to the absolute value error criteria, or $L_1$ norm:

$$\sum_{k=1}^{N} \left| \omega_k^{\pm} \, e_k \right| = \text{minimum} \tag{4}$$

in contrast with the $L_2$ norm which minimizes the sum of the squares of the errors. The term $\omega_k^{\pm}$ in equation (4) is a special weighting function which may be asymmetric about $e_k = 0$. Each row in the inverse problem (1) is assigned two weighting coefficients, one for positive error and the other for negative error. If $\omega_k^{+} = \omega_k^{-}$, this particular equation is a simple equality. However, if one of the weights is made substantially

larger than the other, the positive and negative errors are penalized differently and the corresponding equation becomes an inequality. This asymmetric error capability proves very useful in many applications such as this one, where a large number of inequality constraints are imposed simultaneously on the solution.

In this, as in any inverse problem, difficulties can arise if the number of unknowns exceeds the number of observations, or if the distribution of data is biased in such a way that certain parts of the solution are ill-determined. In these situations, some kind of smoothing condition must be applied in order to ensure a unique solution. The smoothness condition used in this application is a linear depth vs velocity relation. (Since a linear interpolation is used for the $x(p)$ curve between successive points $x(p_i)$ and $x(p_{i+1})$, the corresponding depth vs velocity curve cannot be linear. The smoothness condition applies only to the sample points $p_i$, i.e., $z(1/p_{i-1}) - 2z(1/p_i) + z(1/p_{i+1}) = 0.$) The smoothness condition is applied by simply adding the relevant equations to the system of equations (1) and adjusting the weighting function $\omega^{\pm}$ in such a way that the data constraints always dominate. The necessary adjustment is that the $\omega^{\pm}$ for the linear depth vs velocity relations must be less than the weighting function for the data divided by the total number of linear $z(1/p)$ constraints.

In its final form, the inverse problem contains equations corresponding to five different types of constraint: travel time information, an extremal depth condition, a single valued velocity restriction, p-x bounds, and a smoothness criterion. Clearly, all of these conditions together give us an over-determined system of equations. The $L_1$ algorithm solves this type of problem by selecting $M$ of the $N$ equations to be satisfied

exactly (M is the number of unknowns). We point out that this feature of the $L_1$ solution does not imply that the remaining N-M equations are ignored; the particular set of M equations to be satisfied are selected so as to minimize the cumulative errors from the problem as a whole.

## 4 TRAVEL TIME CONSTRAINTS

The ray parameter p at some range x is related to the travel time curve through a derivative;

$$p = \frac{dT(x)}{dx} \quad . \tag{5}$$

The travel time is therefore simply an area under the p(x) curve

$$T(x) = \int_0^x p(y)\, dy \quad . \tag{6}$$

Since p is not always single valued in x, it is more convenient to conduct the integration in p rather than x. Integration of equation (6) by parts yields

$$T(x) = p \cdot x(p) + \int_{p(x)}^{p_{max}} x(q)\, dq$$

$$= p \cdot x(p) + \tau(p) \tag{7}$$

The delay time $\tau(p)$ represents the time intercept at x = 0 for ray parameter p and travel time T(x). For a discrete p(x) curve, $\tau(p)$ is simply a summation of the source-receiver distances over some interval of ray parameters $[P_i, P_{max}]$ ,

$$\tau_i = \sum_{j=i}^{i_{p_{max}}} x_j \, \Delta p_j \qquad (8)$$

Equation (8) is in the same form as one row of the inverse problem, equation (2). Thus, $\tau(p)$ data can be entered directly into the inverse problem and fitted in one iteration. However, this is not the case for $T(x)$ data. Travel times must be converted to the appropriate integral form using equation (7) before they can be entered into the inverse problem. Note that in equation (7), each $T(x)$ pair requires a corresponding $p$ value in order to set the lower limit of integration. Initial estimates for $p$ at each observation distance $x$ can be obtained by differentiating the $T(x)$ curve. One way to improve these $p$ values is by solving the inverse problem iteratively without the extremal depth condition until the $p(x)$ solution matches the $p$ limit used to evaluate equation (7).

In the inverse problem, $T(x)$ data provide simple integral constraints on the $p(x)$ curve, just as $\tau(p)$ data do. Integral constraints place no restrictions on the individual distances $x_j$, which means that the travel times for the initial solution may not match the observed $T(x)$ values. In other words, the velocity-depth model is not yet consistent with the travel time data. One way to remedy this situation is to place bounds on the $p(x)$ solution. These bounds are determined by comparing the travel times of the inverse solution with those of the observed seismograms. In general, this $p(x)$ envelope must be refined by performing the inverse and forward problems several times, until a satisfactory fit is obtained. The discrepancy between the observed and calculated seismograms depends on the width of the $p(x)$ envelope used to constrain the solution. Thus, two types of constraints are needed to match travel time data. The procedure for

matching travel time data will be illustrated further in the following sections when we present some examples.

If there are any triplications in the observed $T(x)$ data, it is advantageous to use the differential travel times between the early and later arrivals to constrain the $p(x)$ solutions. The differential travel times provide integral constraints over smaller sections of the $p(x)$ curve and therefore provide stronger constraints than do the absolute arrival times. By a similar argument, we expect the extremal velocity-depth limits to reflect the number of integral constraints imposed — in other words, the number of $T(x)$ data used.

## 5 EXTREMAL DEPTH CONSTRAINT

McMechan & Wiggins (1972) and Wiggins, et al. (1973) have shown how the $p(x)$ function can be manipulated in order to obtain maximum and minimum depths corresponding to any given velocity. In this section, we will illustrate how such an extremal depth condition can be incorporated directly into the inverse problem. This will automatically give an extremal earth model which is consistent with the data each time the inversion is performed.

The depth $z(p)$ corresponding to the turning point of ray $p$ is obtained by the Weichert-Herglotz integral of the $p(x)$ curve:

$$z(p) = \frac{1}{\pi} \int_{p}^{p_{max}} \frac{x(q)}{\left(q^2 - p^2\right)^{1/2}} \, dq \quad , \tag{9}$$

where the corresponding velocity is $v = 1/p$. For a discrete $p(x)$ curve, equation (9) becomes

$$z_i = \sum_{j=i}^{i_{p_{max}}} x_j \cdot \int_{p_j}^{p_{j+1}} \frac{dq}{\left(q^2 - p_i^2\right)^{1/2}} \quad , \tag{10}$$

which is simply a weighted summation of the discrete distances $x_j$ over the $p$ interval $[p_i, p_{max}]$. These weighting coefficients are positive and decrease monotonically in $p$. In order to determine the $p(x)$ curve which satisfies the data constraints and gives an extremal depth for some ray parameter $p^*$, say, one row containing the Weichert-Herglotz coefficients for $z(p^*)$ is added to the inverse problem, equation (1). Let's say we wish to minimize the depth for $p^*$. The corresponding depth value in the vector $\bar{d}$ is then set to zero and the asymmetric weighting function $\omega^{\pm}$ for this equation is set to some value less than $\omega^{\pm}$ for the data constraints and larger than the sum of the $\omega^{\pm}$ for the linear $v(z)$ relations. If the weighting function $\omega^{\pm}$ is chosen correctly, the $L_1$ algorithm will find a solution which accomodates for this extremal depth constraint, but does not actually solve it. The data equations will take precedence. Consider the following example.

## 6 MONOTONIC p(x) EXAMPLE

Fig. 1(a) shows three seismograms which were computed from the $p(x)$ curve in Fig. 1(b) using Disc Ray Theory integration. The solid curve in Fig. 1(c) shows the corresponding earth model. These three seismograms provide three travel time data which were used as input data for the inverse problem. The travel times, along with their corresponding $p$ values, are listed in Table 1.

To fix ideas, we first illustrate the set-up of the inverse problem for this example. The ray parameter ranges from .12 to .18 sec/km. If a sampling interval of $\Delta p = .01$ sec/km is used, the inverse problem is set up to estimate six values of $x_j$ (x(.18) is zero):

$$\bar{x} = [x_1, x_2, \ldots x_6]^T . \tag{11}$$

The matrix $\bar{\bar{A}}$ and vectors $\bar{d}$ and $\bar{\omega}^{\pm}$ are

$$\begin{array}{c|cccccc|c|cc}
\text{Row} & & & \bar{\bar{A}} & & & & \bar{d} & \bar{\omega}^- & \bar{\omega}^+ \\
1 & .01 & .005 & & & & & .15 & -1. & 1. \\
2 & .01 & .005 & & & & & .25 & -1. & 1. \\
3 & .01 & .01 & .01 & .005 & & & .75 & -1. & 1. \\
4 & .01 & .01 & .01 & .005 & & & .85 & -1. & 1. \\
5 & .01 & .01 & .01 & .01 & .01 & .005 & 1.75 & -1. & 1. \\
6 & .01 & .01 & .01 & .01 & .01 & .005 & 1.85 & -1. & 1. \\
7 & 1. & & & & & & 0. & -L & \epsilon \\
8 & & 1. & & & & & 0. & -L & \epsilon \\
9 & & & 1. & & & & 0. & -L & \epsilon \\
10 & & & & 1. & & & 0. & -L & \epsilon \\
11 & & & & & 1. & & 0. & -L & \epsilon \\
12 & & & & & & 1. & 0. & -L & \epsilon \\
13 & -.011 & .075 & & & & & 0. & -L & \epsilon \\
14 & -.021 & -.011 & .077 & & & & 0. & -L & \epsilon \\
15 & -.007 & -.021 & -.012 & .080 & & & 0. & -L & \epsilon \\
16 & -.004 & -.007 & -.022 & -.012 & .083 & & 0. & -L & \epsilon \\
17 & -.003 & -.004 & -.008 & -.023 & -.012 & .086 & 0. & -L & \epsilon \\
18 & -.252 & .203 & & & & & 0. & -.001, & .001 \\
19 & -.020 & -.231 & .185 & & & & 0. & -.001, & .001 \\
20 & .035 & -.018 & -.210 & .168 & & & 0. & -.001, & .001 \\
21 & .008 & .032 & -.016 & -.189 & .151 & & 0. & -.001, & .001 \\
22 & .003 & .007 & .028 & -.014 & -.170 & .134 & 0. & -.001, & .001 \\
23 & .029 & .034 & .043 & .068 & .083 & & 0. & -.01 , & .01
\end{array} \tag{12}$$

The precedence of each equation is determined by its corresponding weighting function $\omega_i^{\pm}$. Here $L$ and $\varepsilon$ are very large and small numbers, respectively, which serve to make the corresponding equations into inequalities. Rows 1 through 6 impose the travel time observations. Notice that each observation is entered twice in order to incorporate the range of uncertainty in the observation. Rows 7 through 12 impose the condition $x_i \geq 0$. Rows 13 through 17 impose the condition that $z$ be single valued in $V$, i.e., $z_i \geq z_{i-1}$. The coefficients for these rows were obtained by taking the first differences of the Weichert-Herglotz coefficients defined in Equation (10). Rows 18 through 22 suggest that in the absence of other constraints, the velocity depth function should be linear. These rows were obtained by taking second differences of the Weichert-Herglotz coefficients. Finally, the last row requests that the solution minimize the depth corresponding to $p = .13$ sec/km.

The Weichert-Herglotz weighting coefficients for $p = .13$ sec/km are shown in Fig. 1(b). (A sampling interval of $\Delta p = .005$ sec/km was used for these calculations.) The minimum depth condition for $p = .13$ requires that the weighted sum of the solution $x_j$ over the $p$ interval [.13, .18] be zero, since the corresponding depth value in the $\bar{d}$ vector has been set to zero. To obtain the velocity model which gives a maximum depth for $p = .13$ sec/km, the inverse problem is solved with a very large depth value in the data vector $\bar{d}$. The $p(x)$ curves which give the maximum and minimum depths are shown in Fig. 1(b). In the region around $p = .13$ sec/km, the solutions behave as would be expected, considering the nature of the extremal depth constraints. At about $p = .15$ and $p = .125$ sec/km, the two solutions cross one another. This is because the three travel times constrain the areas under the $p(x)$ curves over the

intervals [.16, .18], [.14, .18], [.12, .18] and the large excursions at $p = .13$ sec/km must be compensated elsewhere. The velocity-depth models show a similar cross-over behavior. The solution which minimizes the depth at $p = .13$ sec/km has maximum depths at $p = .16$ and $p = .12$ sec/km. However, the depths for ray parameters other than .13 sec/km are not necessarily extremal. We have determined only two of all the possible earth structures consistent with these data constraints. The $v(z)$ envelope which encompasses all these models is obtained by repeating the inverse problem with extremal depth conditions applied to each discrete $p_j$ in turn.

Note that both $v(z)$ solutions in Fig. 1(c) have regions where $z$ is constant in $v$. This shows that the single-valued velocity criterion, which was imposed as an inequality equation, was actually solved as an equality in the final solutions. Without this constraint, the $v(z)$ functions would not be physically meaningful. The single-valued velocity condition controls the shape of the reverse branches $\left(\frac{dp}{dx} > 0\right)$ of the $p(x)$ functions. The small irregularities in the reverse branches are due to the discrete nature of the Weichert-Herglotz integral. Note that some of the linear $v(z)$ relations are also satisfied in the final solutions. The linear portions of the $v(z)$ curves correspond to the forward branches $\left(\frac{dp}{dx} < 0\right)$ of the $p(x)$ curves.

The travel time curves and synthetic seismograms for the two extremal earth models are presented in Fig. 1(d). The calculated travel times are not consistent with the "observations" because we have not used an envelope to limit the individual distances $x_j$. So far, we have only placed integral

constraints on the $p(x)$ curves, which is, in effect, the same as using three $\tau(p)$ data. At those points on the travel time curves in Fig. 1(d) where the slopes are .16, .14 or .12 sec/km, the corresponding delay time values are correct. However, the $T(x)$ values are incorrect because these slopes do not occur at distances of 20, 40 or 60 km, as they should.

Fig. 2 shows the solutions which maximize the minimize the depths for each discrete ray parameter between $p = .12$ and $p = .16$ sec/km, with $\Delta p = .005$ sec/km. The only difference between each of these solutions is in the row containing the Weichert-Herglotz coefficients in the inverse problem. The width of the $v(z)$ envelopes in Fig. 2(b) changes substantially with $p$. This behavior is controlled by the $p$ limits on the travel time integrals. The $v(z)$ envelope is narrower for $p$ values close to these limits. Many of the velocity-depth models cross from one extremal limit to the other for different values of $p$. Note, however, that one particular solution cannot exhibit maximum or minimum depths for <u>every</u> $p$, since this would violate the travel time integrals.

## 7 EFFECTS OF OBSERVATIONAL ERRORS AND NUMBER OF DATA

Intuitively, we expect the width of the velocity-depth envelope to reflect the amount of uncertainty associated with each data point. Observation error can be incorporated into the inverse problem in the following manner: First, an estimate of the uncertainty $\pm \Delta d_k$ associated with each data value $d_k$ is made. For example, in the previous problem, each travel time observation was assigned an uncertainty of $\pm$ .05 sec. Then, two equations for each data constraint are simultaneously added to the inverse problem; one containing the value $(d_k + \Delta d_k)$ and the other with $(d_k - \Delta d_k)$ in the data vector $\overline{d}$. The extremal depth constraint causes

the final error in the $L_1$ algorithm to be minimized at either one of the endpoints. The algorithm automatically selects the best equation to be exactly satisfied. In general, the minimum depth solution selects the one endpoint and the maximum depth solution the other. Hence, the larger the uncertainty in the data, the greater the difference between the two solutions. The effect of data uncertainty in the previous problem can be seen in Fig. 2(b), where the $v(z)$ envelope for travel time uncertainties of $\pm$ .1 sec. is also shown. However, since the widths of the two $v(z)$ envelopes are nearly identical, we can conclude that the large depth limits in this example are caused by factors other than observation error.

The next example shows how the number of observations affects the resolution of earth structure. It is essentially a repeat of the previous problem, except that six travel time constraints are used. Their associated p values are .12, .13, .14, .15, .16 and .17 sec/km. Again, extremal depthts for each discrete ray parameter $p_j$ in the interval [.12, .16] are found in turn. The solutions are presented in Fig. 3. The range in velocity-depth models is much smaller than in the previous example. In particular, the number of "steps" in the $v(z)$ envelope has increased. The $T(x)$ and $p(x)$ solutions are also better behaved than the ones in Fig. 2. However, there is still a considerable discrepancy between the observed and calculated travel times. The next step in the interpretation scheme is to limit the $p(x)$ solutions in such a way that the corresponding velocity-depth models become consistent with the observed seismograms.

## 8 MATCHING THE OBSERVED SEISMOGRAMS

In order to depict accurately the range of earth structures consistent with a given data set, the inverse problem requires more than simple linear constraints on the $p(x)$ curve. As we saw in the previous examples, the arrivals corresponding to the initial $p(x)$ solutions have travel times and amplitudes which are radically different from the observed seismograms. Travel time inconsistencies can be eliminated by constructing bounds in the $p$-$x$ plane and thereby restricting the range of allowable travel time integrals for the $p(x)$ solutions. For example, the travel time for a synthetic arrival which occurs earlier than indicated by the observed data can be increased in the next iteration by imposing bounds which limit the minimum values attained by the $p(x)$ solutions.

Amplitude information is also incorporated into the inverse problem through the $p(x)$ envelope. The objective is to make the amplitudes of the synthetic seismograms match the amplitude vs distance behaviour of the recorded data. The $p(x)$ envelope is used to restrict the slopes of the $p(x)$ solutions and to control the locations and lateral extensions of any triplications. Since recorded seismograms usually exhibit a "scatter" in amplitude between adjacent traces, an attempt is made to match only those amplitude-distance variations which can be attributed to gross changes in the velocity-depth function.

The strategy for matching the travel times and amplitudes of the observed seismograms is interactive. The first step is to obtain a set of extremal solutions with no $p(x)$ envelope constraint. We then examine the synthetic seismograms corresponding to each of the solution models. Some of the synthetic arrivals will be consistent with the observations and some will not. If we were to color the sections of the $p(x)$ curves that correspond to inconsistent arrivals, we would conclude that certain portions of the $p$-$x$ plane should be excluded in order to obtain the desired time-amplitude behaviour. If we then incorporate such limits on the $p(x)$ solutions, we can perform another iteration and continue this process until all of the models have a satisfactory distribution of arrivals.

Obviously, this approach is fairly crude. There may be types of amplitude variations that are not simply correlated with areas in the $p$-$x$ plane. The approach used here could not address such possibilities. Our experience from initial applications of this technique is that the use of $p(x)$ limits has handled the incorporation of amplitudes to the degree that we are willing to trust the amplitude variations.

To illustrate the effects of the $p(x)$ envelope constraint, the $T(x)$ data in Table 1, which were used as data constraints for the solution in Fig. 2, have been inverted with limits on the $p(x)$ curves. The results are presented in Fig. 4. Two things are immediately obvious: The $v(z)$ envelope is much narrower than the one in Fig. 2(b) and the synthetic seismograms are now very similar to the "observed" seismograms in Fig. 1(z). The spurious arrivals have been completely eliminated. Again, maximum and minimum depths for $p$ only in the range $p = .12$ to $p = .16$ sec/km have

been determined. Also shown in Fig. 4(b) are the extremal depth limits for a slightly wider $p(x)$ envelope. There is a close relationship between the width of the $p(x)$ envelope and the range of allowable earth models.

## 9 TRIPLICATION EXAMPLE

The next example is more realistic. Fig. 5(a) shows four seismograms computed from the $p(x)$ curve in Fig. 5(b). The earth model has a high velocity gradient at a depth of about 10 km which causes a triplication in the $p(x)$ and $T(x)$ curves. This example is different from the previous one because all of the arrivals have associated $p$ values which fall on the forward branches ($dp/dx < 0$) of the $p(x)$ curve. These regions of the $p(x)$ curve are therefore quite well constrained while the solutions of the range $p = .14$ to .16 sec km are under-constrained. Fig. 6 shows the extremal depth solutions for each discrete ray parameter between $p = .12$ and .18 sec/km. The uncertainty in the solutions is strongly dependent on $p$. The $v(z)$ envelope in Fig. 6(b) shows no indication of the large velocity gradient at 10 km depth. However, the $T(x)$ curves in Fig. 6(c) do indicate the presence of a triplication. Also shown in Fig. 6(b) is the $v(z)$ envelope obtained when the differential travel time constrains are omitted. These data have a significant effect on the width of the velocity-depth limits.

Fig. 7 shows the extremal depth solutions obtained using the same data as above with an envelope limiting the $p(x)$ curves. The range in $v(z)$ models is decreased considerably relative to the results in Fig. 6(b). The travel times and amplitudes are now quite similar to the "observations" in Fig. 5(z). Even though the $p(x)$ envelope here is quite narrow, there are still some obvious discrepancies between the observed and calculated travel times of the second arrivals. Thus, the $p(x)$ limits could be made even narrower. Also presented in Fig. 7(b) is the $v(z)$ envelope obtained by using a slightly wider $p(x)$ envelope.

## 10 OFFSHORE EXAMPLE

As a final example, we present the results of our interpretation scheme applied to oceanic crustal data from Spudich, et al. (1979). These data have been interpreted by Spudich, et al. (1979) by matching the waveforms of the observed seismograms and synthetics computed using the reflectivity method. They have also interpreted these data using the travel time inversion scheme of Garmany, et al. (1979). This technique uses linear programming to invert for a velocity-depth distribution directly from a $\tau(p)$ envelope. Fig. 8 shows the final solutions obtained by applying our interpretation scheme to the same $\tau(p)$ data used by Spudich, et al. (1979). The $p(x)$ solutions have been forced to lie within a narrow envelope in order to match the first arrival times and amplitudes of the observed data. The travel times for the later arrivals could not be determined from the observed seismograms with any reasonable accuracy and so are not shown. Because these data are lacking, the amplitude information is essential for determining the nature of the triplications in this example. The relative amplitudes shown in Fig. 8(d) are the maximum displacements for each of the observed seismograms and for synthetics which were computed from the $p(x)$ solutions using Disc Ray Theory integration.

Fig. 8(e) shows the velocity models for the offshore data obtained by Spudich, et al. (1979) and by our interpretation method. The depth limits obtained using the travel time inversion scheme of Garmany, et al. (1979) are somewhat larger than those obtained using our procedure in the first iteration (e.g., without a $p(x)$ envelope). We have attributed this discrepancy to two factors; the travel time inversion scheme of Garmany, et al. (1979) does not utilize an explicit smoothing constraint such as a linear velocity-depth

relationship, and the earth model used by Spudich, et al. (1979) for their inverse problem had more degrees of freedom than ours did.

## 11 DISCUSSION

We have presented a technique for interpreting body-wave seismograms which involves modifying the $p(x)$ curve until a best fit is obtained for travel times and amplitudes. The $p(x)$ function is represented by the discrete distances $x_j$, $j = 1, M$ corresponding to finite samplings of the ray parameter, $p_j$, $j = 1, M$. Up to this point we have not mentioned any criterion for choosing a sampling interval $\Delta p$. Ideally, the discretization of the $p(x)$ curve should not affect the solutions. In other words, the sampling interval should be small enough to make the $p(x)$ curve appear continuous. In practice, the number of degrees of freedom in the inverse problem is limited by computer time. The computing effort for the inverse problem is proportional to $NM^3$, where $M$ is the number of unknowns and $N$ is the number of rows in the transfer matrix $\bar{\bar{A}}$. An upper bound for $\Delta p$ for each problem is determined by the complexity of the $p(x)$ curve. The linear interpolation of $p(x)$ is an implicit smoothing constraint which increases in significance as the sampling interval is increased. In general, $\Delta p$ should vary as a function of $p$. In the examples presented above, the sampling interval was deliberately kept large in order to keep the diagrams readable.

We feel that there are two aspects of this interpretation procedure which require additional research. The first involves extending the scheme to include earth structures containing low-velocity zones. The second is related to the method for determining the $p(x)$ envelope, which, at the present time, requires human intervention. We found that one quickly learns how to manipulate the $p(x)$ curve in order to effect desired changes

in the travel times and amplitudes of the synthetic seismograms. However, with some additional programming, this step could be made automatic.

ACKNOWLEDGEMENTS

The authors would like to thank Dr. J. A. Orcutt for supplying the offshore data. We also thank Dr. G. A. Frazier for his critical reading of this manuscript. This research has been supported by the Office of Naval Research under Contract Number N00014-78-C-0061.

REFERENCES

Bessonova, E. N., V. M. Fishman, V. Z. Ryaboyi & G. A. Sitnikova, 1974. The tau method for inversion of travel times — I. Deep seismic sounding data, Geophys. J. R. astr. Soc., 36, 377-398.

Bessonova, E. N., V. M. Vishman, M. G. Shnirman, G. A. Sitnikova & L. R. Johnson, 1976. The tau method for the inversion of travel times — II. Earthquake data, Geophys. J. R. astr. Soc., 46, 87-108.

Claerbout, J. F., & F. Muir, 1973. Robust modeling with erratic data, Geophysics, 38, 826-844.

Garmany, J., J. A. Orcutt, & R. L. Parker, 1979. Travel time inversion: A geometrical approach, J. Geophys. Res., in press.

McMechan, G. A. & R. A. Wiggins, 1972. Depth limits in body wave inversions, *Geophys. J.R. astr. Soc.*, 28, 459-473.

Mellman, G. R., 1978, A method for wave-form inversion of body-wave seismograms, Ph.D. thesis, Seismo. Lab., Calif. Inst. Tech., Pasadena, California.

Spudich, P.K.P., & J. A. Orcutt, 1979. Petrology and porosity of an oceanic crustal site: Results from shear waves, J. Geophys. Res., in press.

Wiggins, R. A., G. A. McMechan & M. N. Toksöz, 1973. Range of earth structure implied by body wave observations, Rev. Geophys. Space Phys. 11, 87-113.

Wiggins, R. A., 1976. Body wave amplitude calculations — II, Geophys. J.R. astr. Soc., 46, 1-10.

TABLE CAPTIONS

Table 1. Travel time data for the three seismograms in Fig. 1(a).

Table 1

| x (km) | T (sec) | P (sec/km) |
|---|---|---|
| 20 | 3.4 $\pm$ .05 | .16 |
| 40 | 6.4 $\pm$ .05 | .14 |
| 60 | 9. $\pm$ .05 | .12 |

FIGURE CAPTIONS

Figure 1. Two solutions to the inverse problem which give extremal depths for one velocity. (a) shows three seismograms which provide the data for the inversion. The solid circles represent travel time uncertainties of $\pm$ .05 sec. The seismograms were computed from the monotonic $p(x)$ function in (b) (solid curve) which has a corresponding earth model depicted as a solid curve in (c). The Weichert-Herglotz coefficients for $p = .13$ used in the extremal depth condition are shown schematically as solid circles in (b). The short and long dashed curves in (b) are the $p(x)$ solutions which minimize and maximize respectively the depth for $p = .13$ sec/km. (c) shows the corresponding velocity-depth models. The $T(x)$ curves and synthetic seismograms for the extremal depth solutions are presented in (d). Note that that travel times and amplitudes for these solutions are not consistent with the data.

Figure 2. Extremal depth solutions for each discrete ray parameter between .12 and .16 sec/km. The data consist of three travel times with uncertainties of $\pm$ .05 sec, as for the results in Fig. 1. The dashed curves in (b) represent the depth limits obtained by using three travel time data with uncertainties of $\pm$ .1 sec. Note the discrepancies between the $T(x)$ curves in (c) and the data in Fig. 1(a).

Figure 3. Extremal depth solutions for six travel time data with uncertainties of ± .05 sec. The "true" earth model for this example is the solid v(z) curve in Fig. 1(c). The only difference between the solutions presented here and those in Fig. 2 is in the number of travel time data used to constrain the p(x) functions. Note that the extremal depths in (b) are much narrower than the ones obtained using three T(x) data, presented in Fig. 2(b). The dashed curves in (b) represent the depth limits obtained by using travel time uncertainties of ± .1 sec.

Figure 4. Extremal depth solutions for the three travel time data in Fig. 1(a) with a p(x) envelope constraint added. The T(x) data have uncertainties of ± .05 sec. The v(z) envelope in (b) is much narrower than the one obtained without using a p(x) envelope, presented in Fig. 2(b). The travel times and synthetic seismograms in (c) are quite similar to the data in Fig. 1(a). The dashed curves in (b) are the depth limits obtained by using the p(x) envelope shown as a dashed curve in (a).

Figure 5. (a) shows four seismograms which provide the data for the "triplication" example. The "true" p(x) and v(z) functions are presented in (b) and (c). The travel time uncertainties are ± .05 sec.

Figure 6. Extremal depth solutions for the travel time data in Fig. 5(a). No envelope was used to restrict the $p(x)$ curves. The data constraints for these results consist of four first arrival times and two differential travel times. The depth limits shown as dashed curves in (b) were obtained using the four first arrival time constraints only.

Figure 7. Extremal depth solutions for the data in Fig. 5(a) with a $p(x)$ envelope constraint added. Note how narrow the depth limits in (b) are compared to those obtained without using a $p(x)$ envelope (Fig. 6(b)). The first arrival times for the above solutions are comparable to the "observed" values in Fig. 5(a) However, the $p(x)$ envelope must be made even narrower in order to fit the travel times for the later arrivals. The dashed curves in (b) represent the depth limits obtained by using the dashed $p(x)$ envelope in (a).

Figure 8. Results obtained by inverting oceanic crustal data. The $v(z)$, $p(x)$, $T(x)$ and amplitude functions obtained in the final iteration are presented as solid curves in (a), (b), (c) and (d) respectively. The final $p(x)$ envelope for these solutions can be seen in (b). The first depth to be maximized occurs at $v = 4$ km/sec and the next one is at 5.9 km/sec. Between 5.9 and 8 km/sec the velocity increments are quite small. The solid circles in (c) represent the errors for the observed

(Figure 8 continued)

travel times. The maximum amplitudes for the observed seismograms are depicted as solid circles in (d). (e) shows the depth limits obtained by the travel time inversion scheme of Garmany, et al. (1979) ("+"'s) and by our technique, with and without using the $p(x)$ *envelope constraint* (*long dashed and* solid curves respectively). The layered crustal model obtained by Spudich, et al. (1979) by waveform fitting is shown in (e) as a short dashed curve.

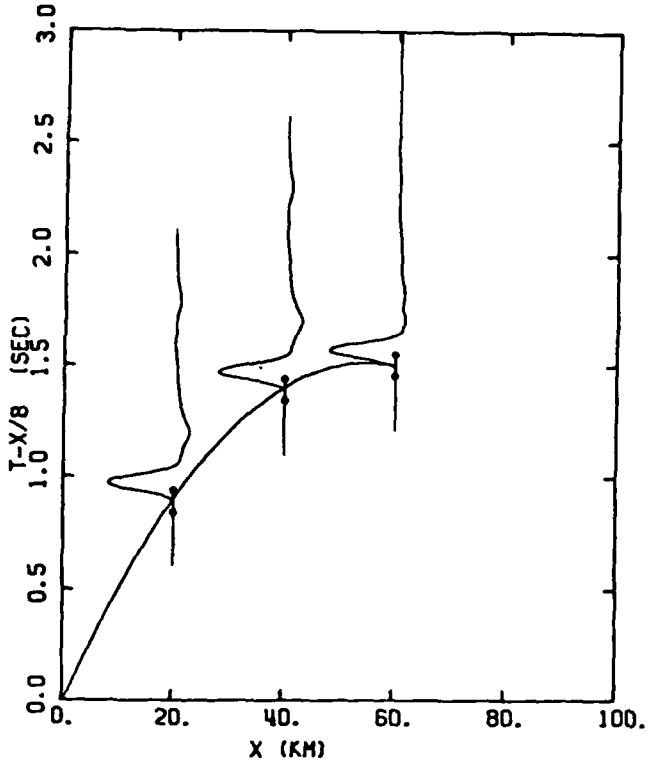


Figure 1(a)

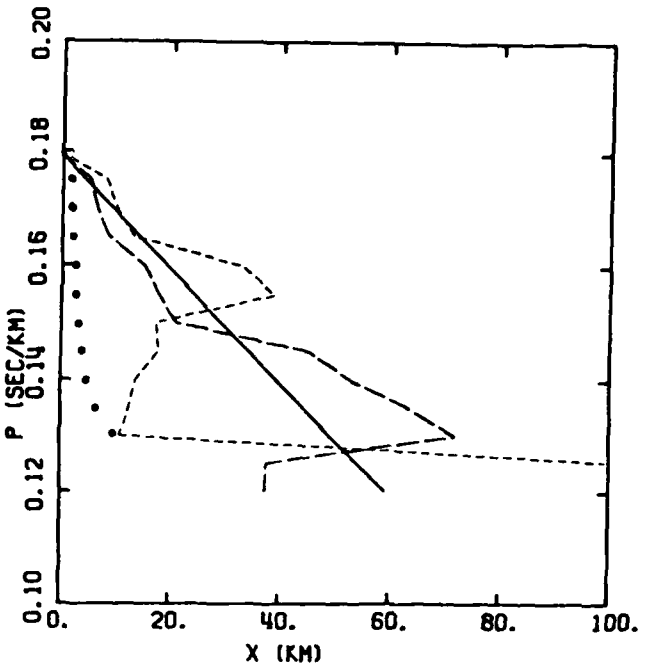


Figure 1(b)

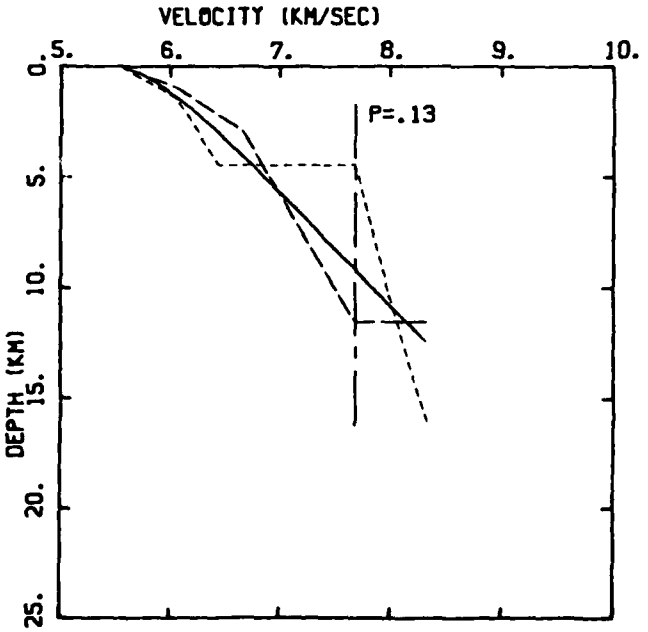


Figure 1(c)

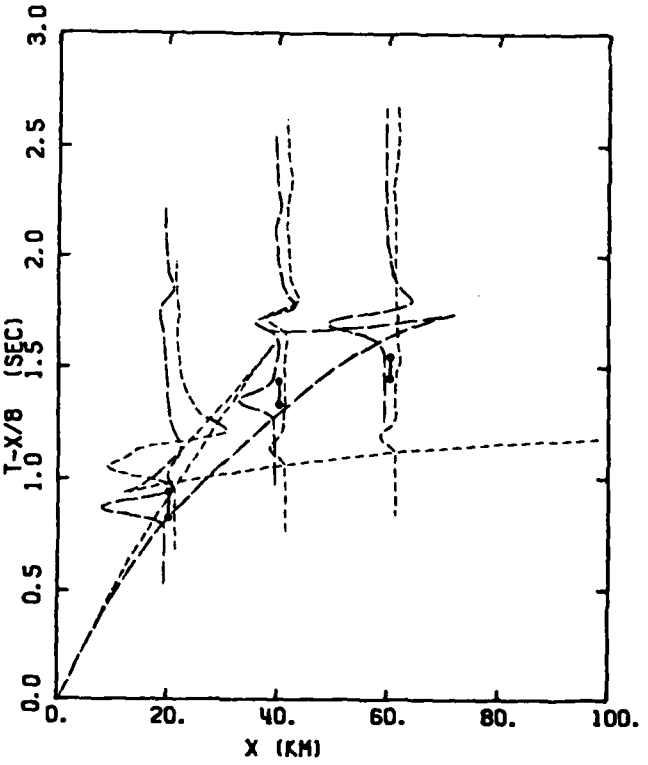


Figure 1(d)

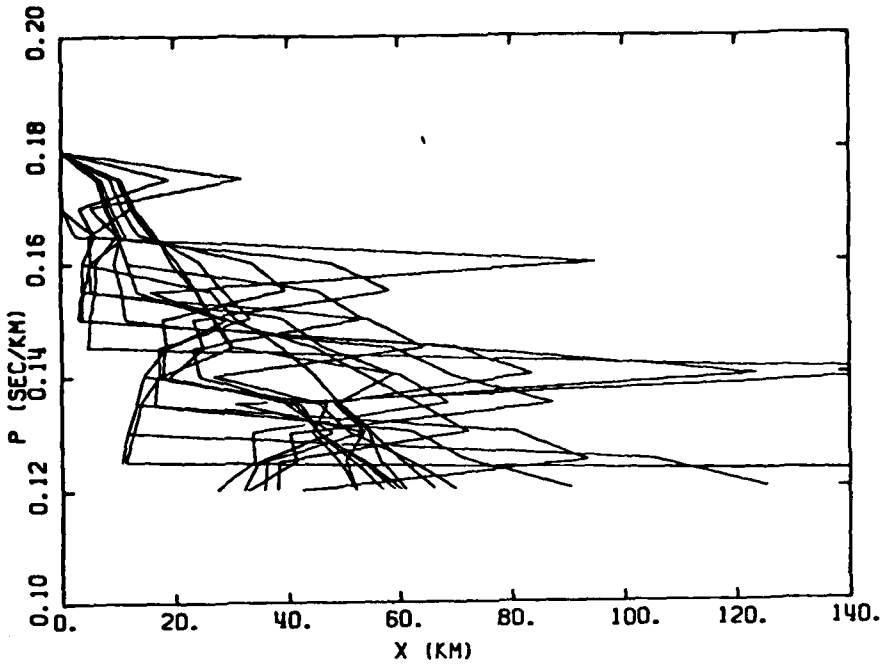


Figure 2(a)

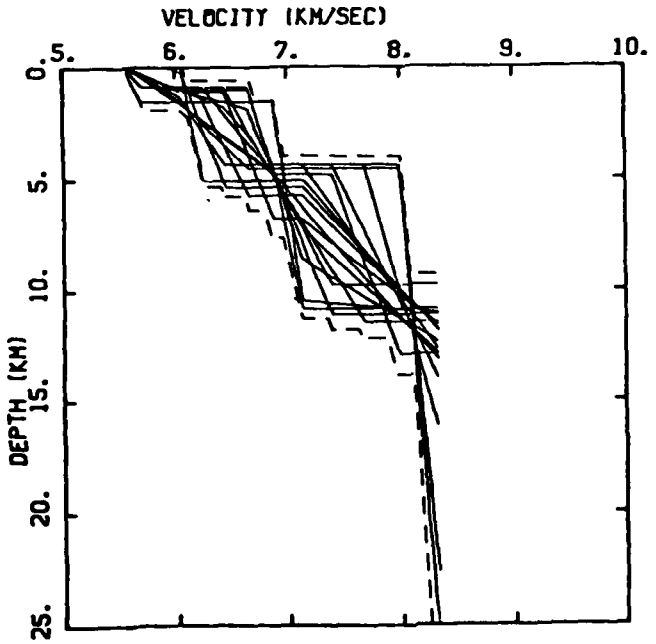


Figure 2(b)

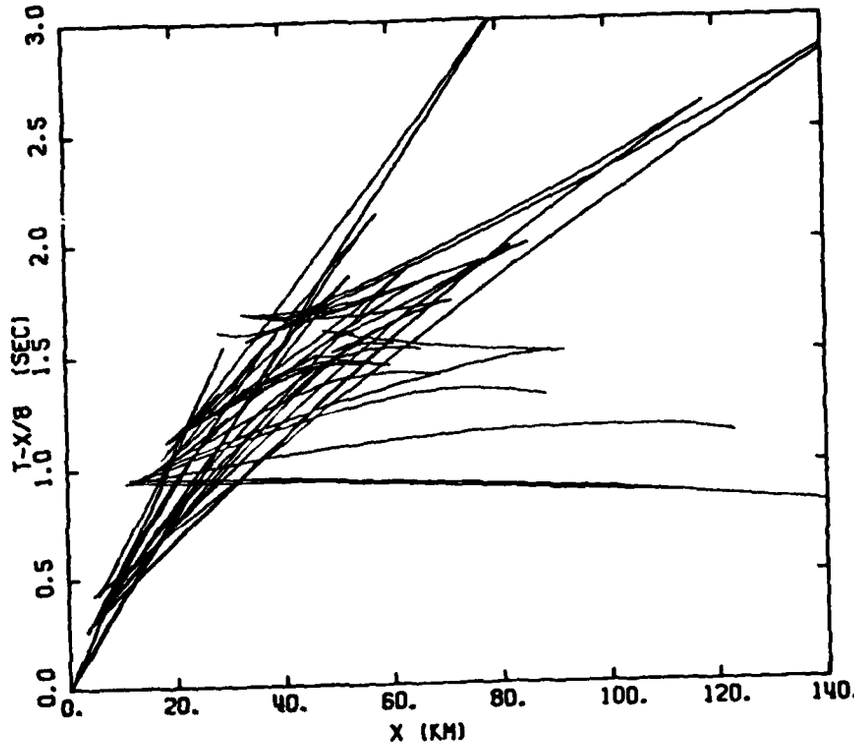


Figure 2(c)

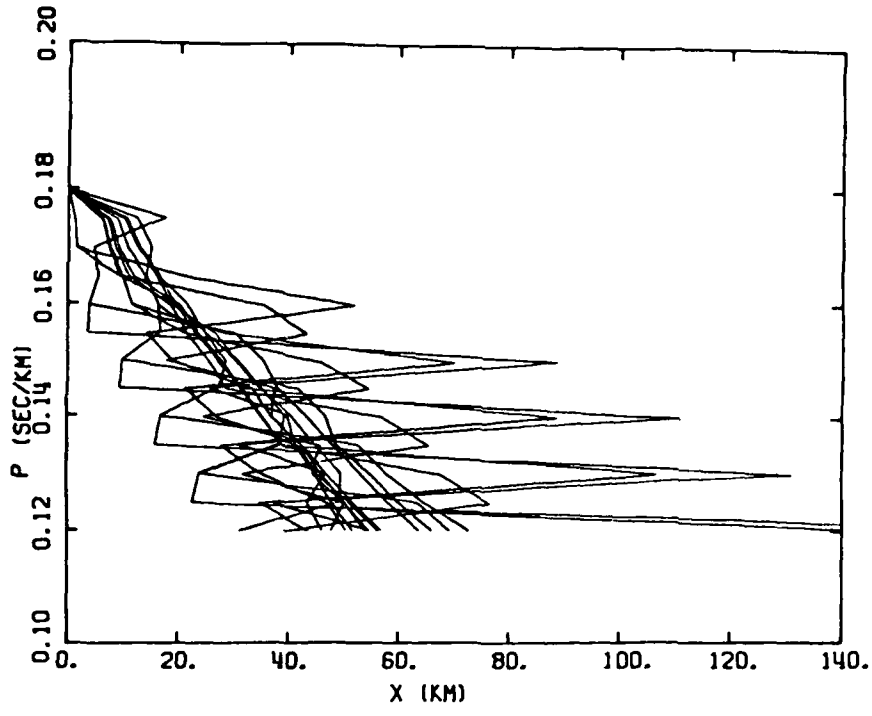


Figure 3(a)

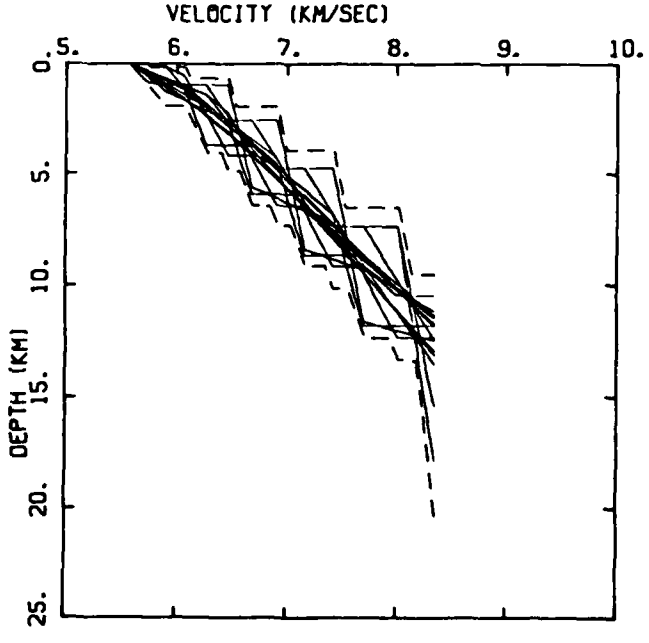


Figure 3(b)

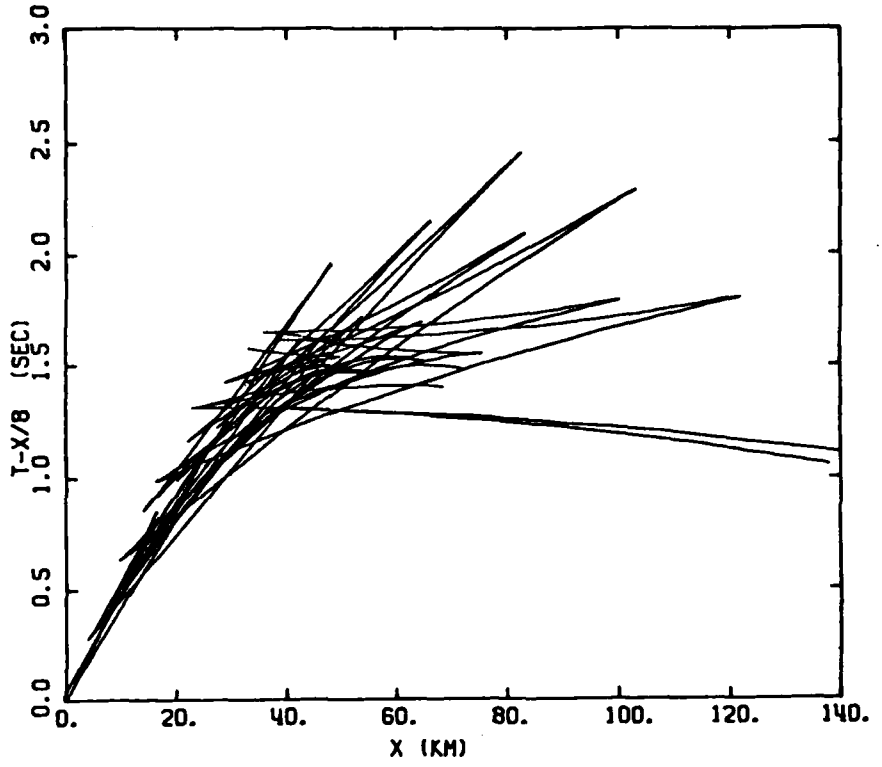


Figure 3(c)

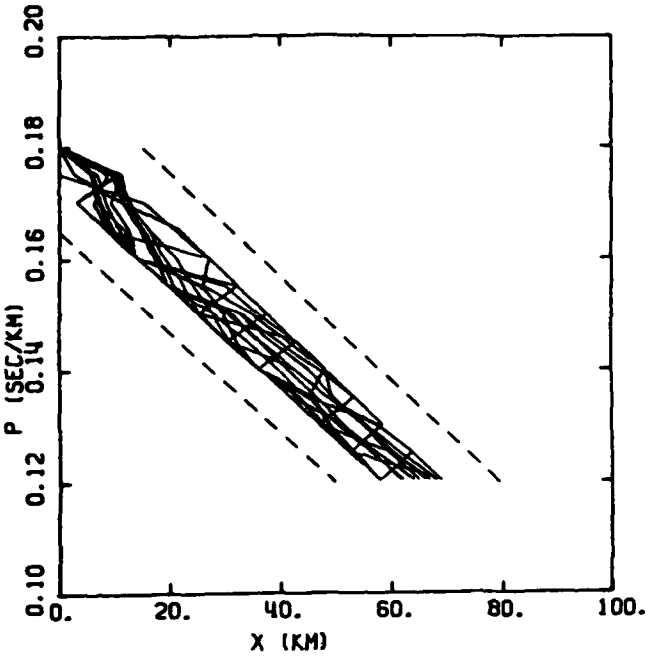


Figure 4(a)

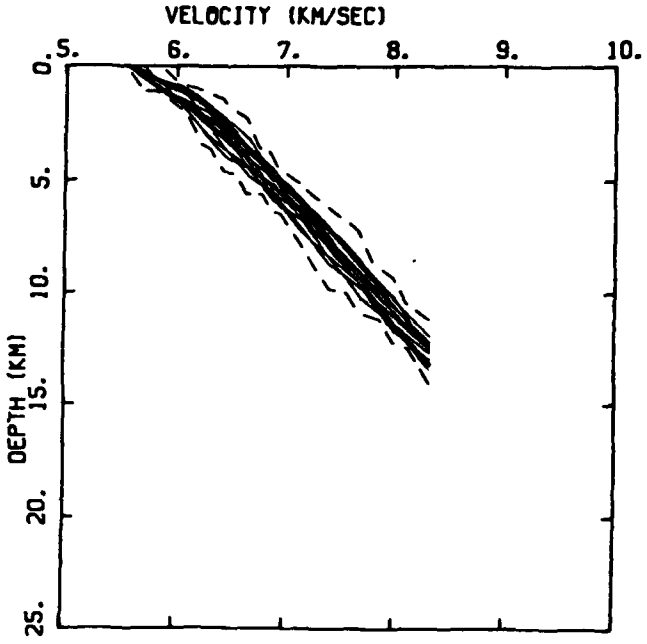


Figure 4(b)

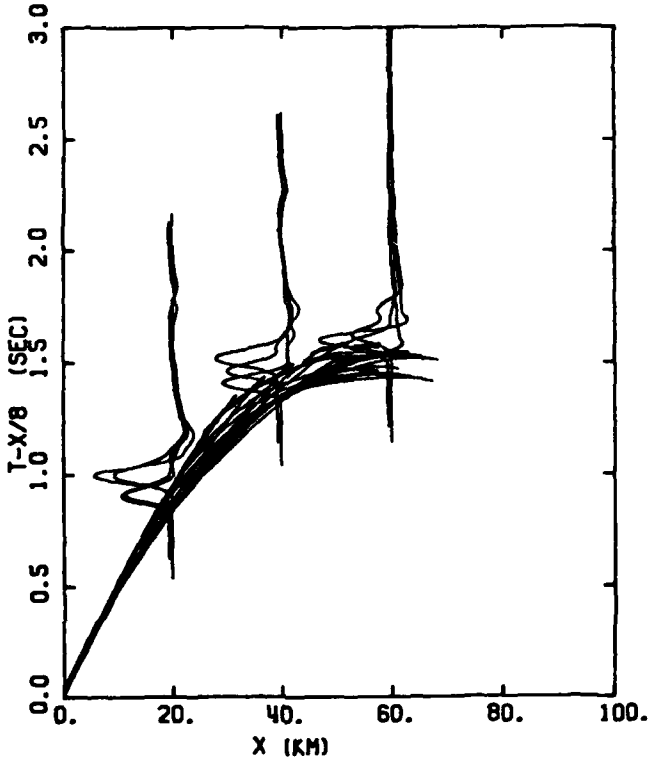


Figure 4(c)

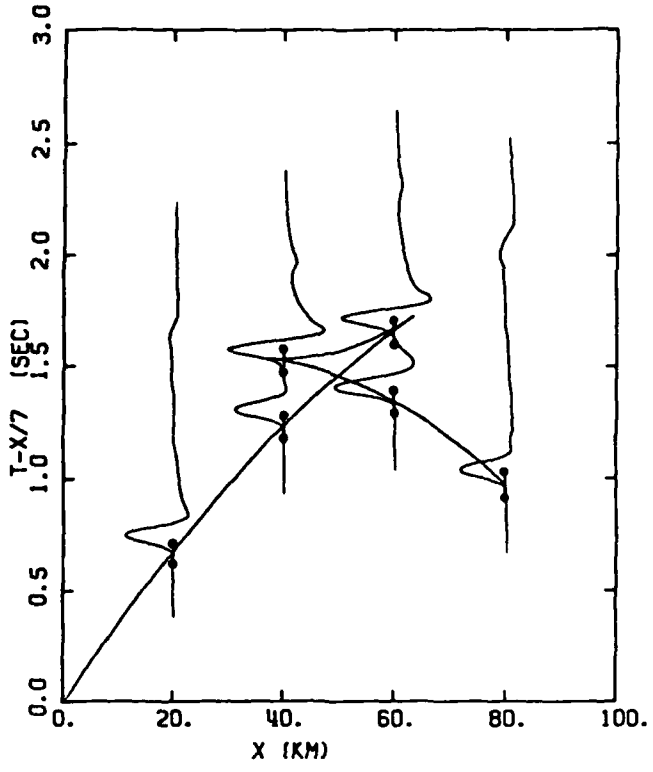


Figure 5(a)

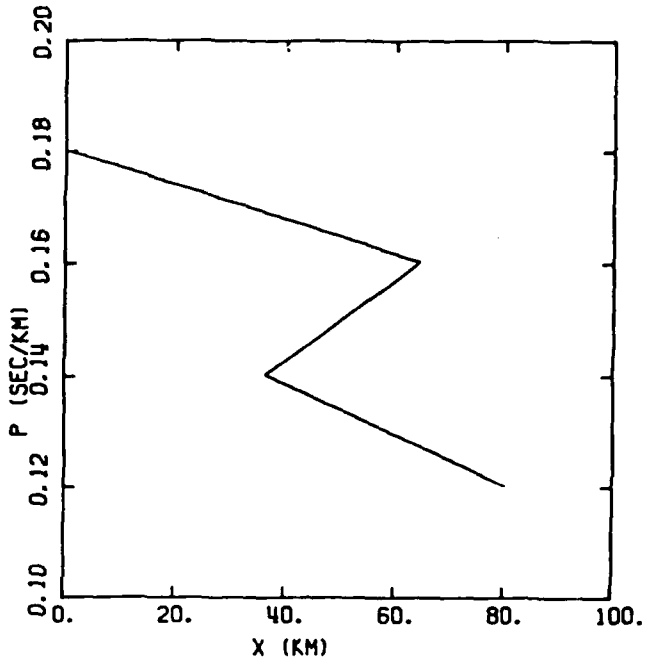


Figure 5(b)

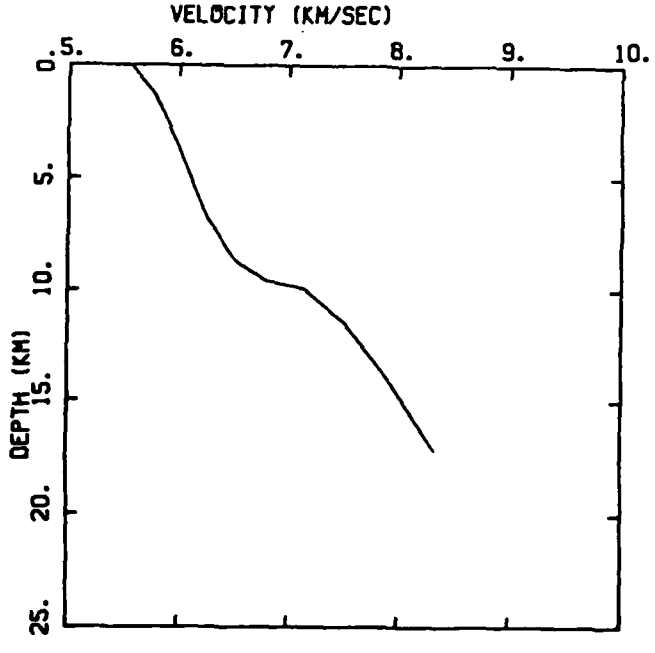


Figure 5(c)

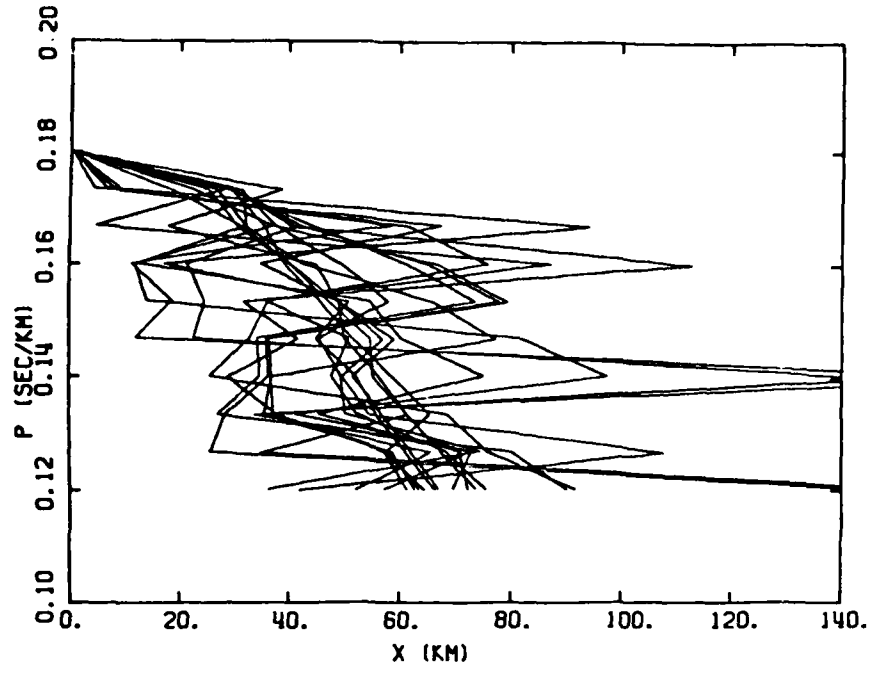


Figure 6(a)

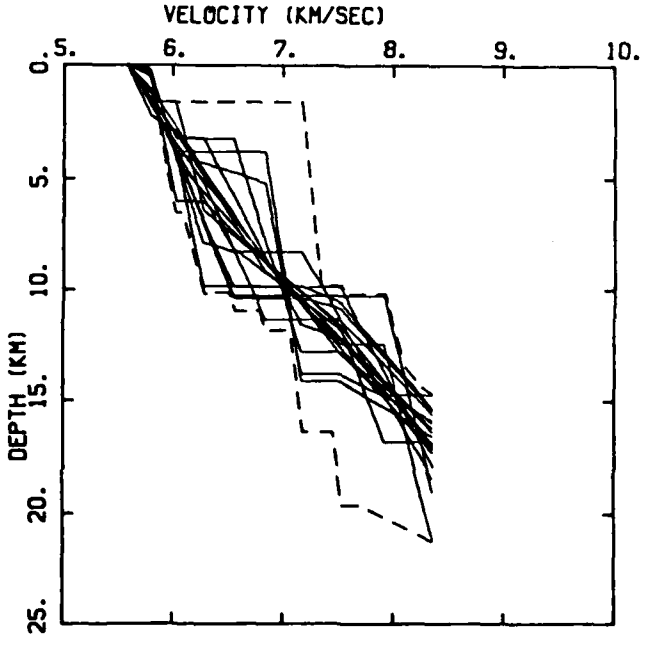


Figure 6(b)

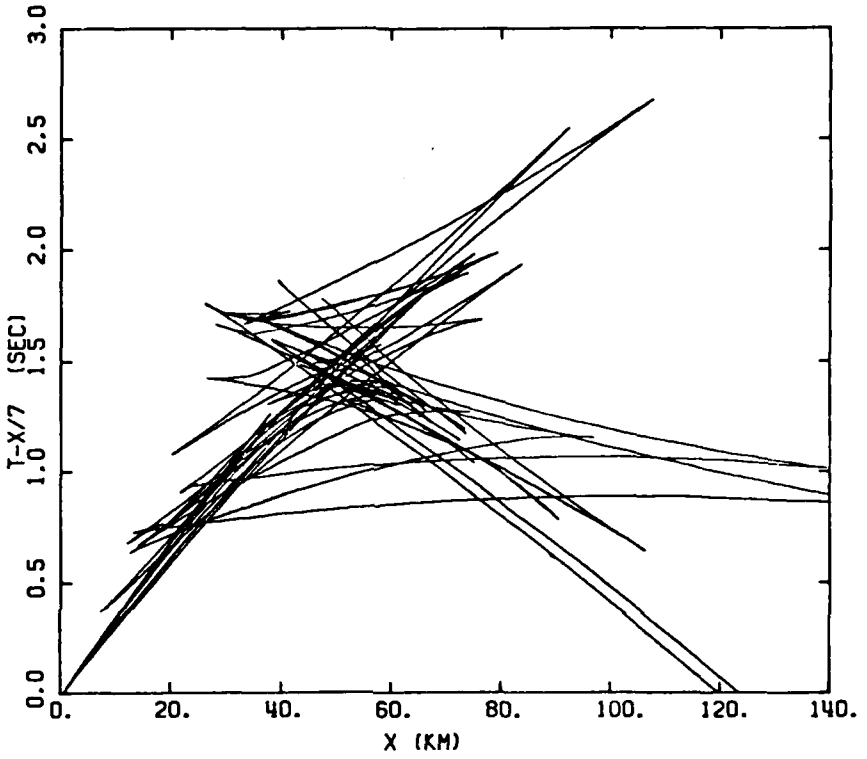


Figure 6(c)

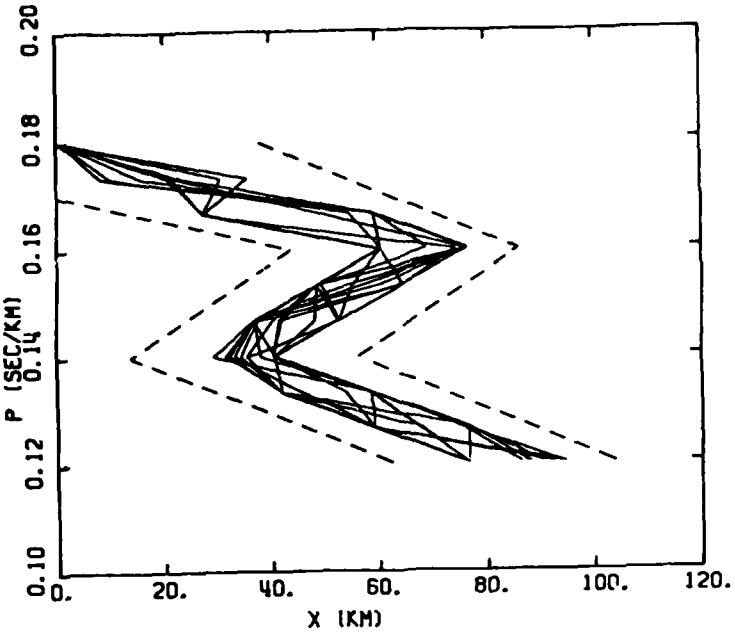


Figure 7(a)

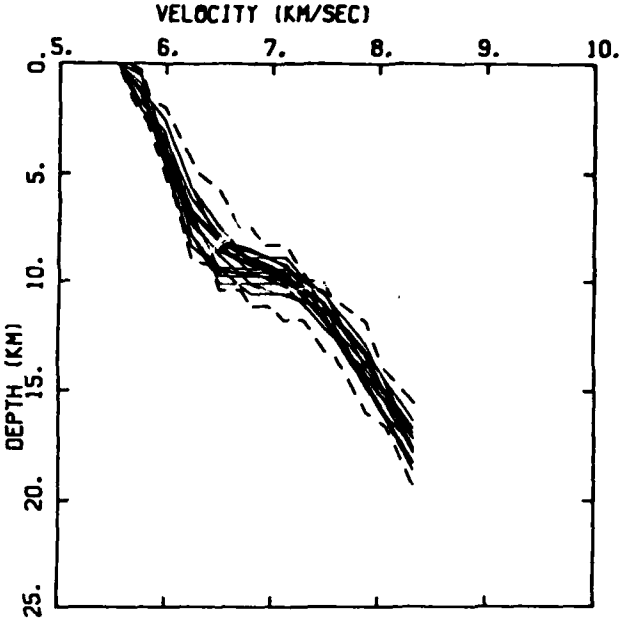


Figure 7(b)

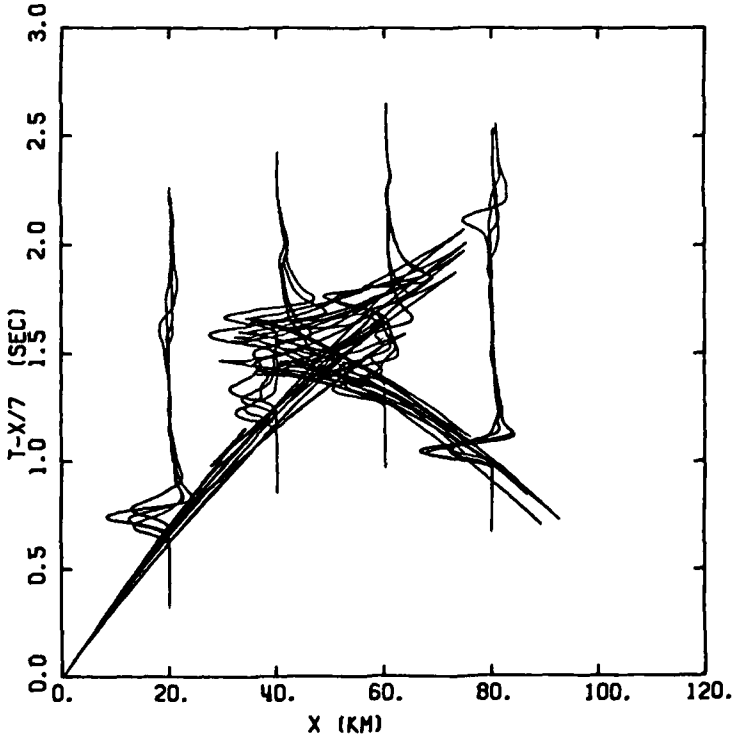


Figure 7(c)

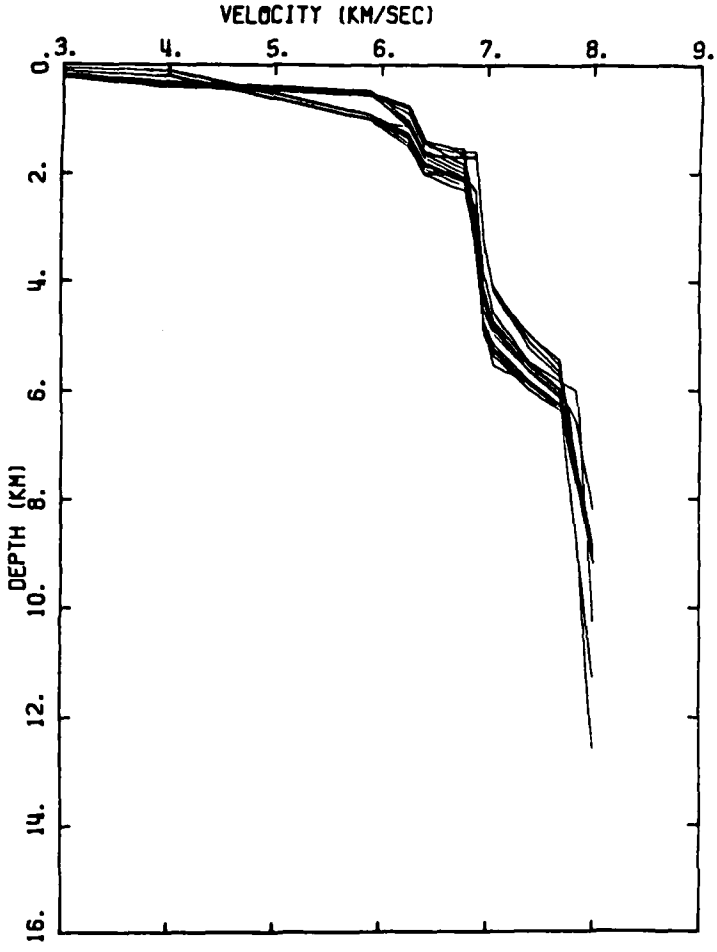


Figure 8(a)

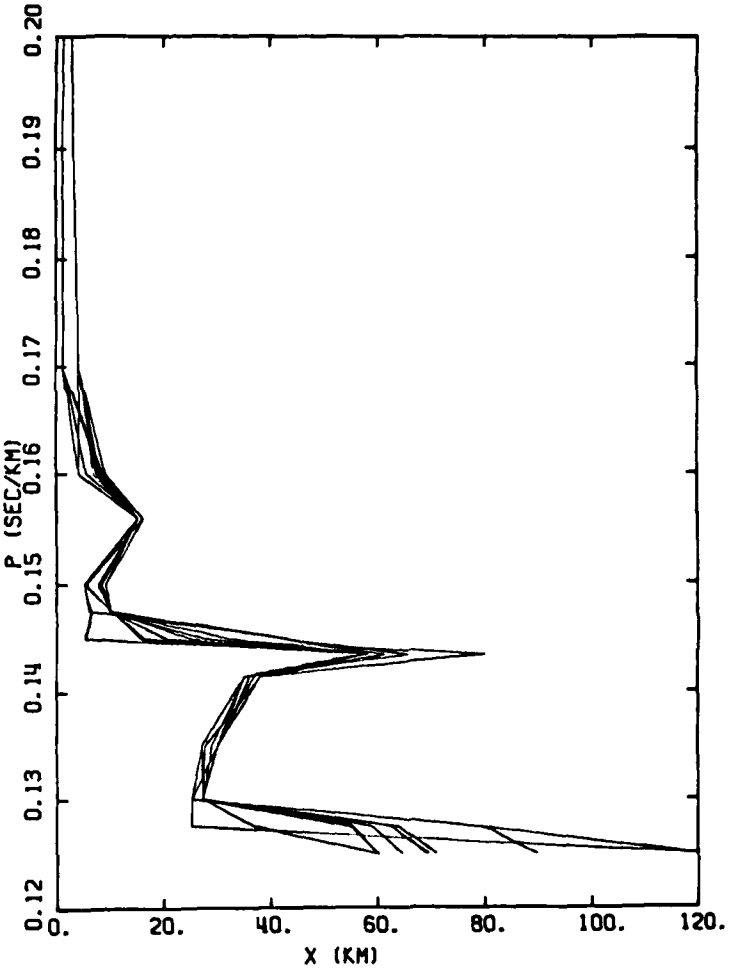


Figure 8(b)

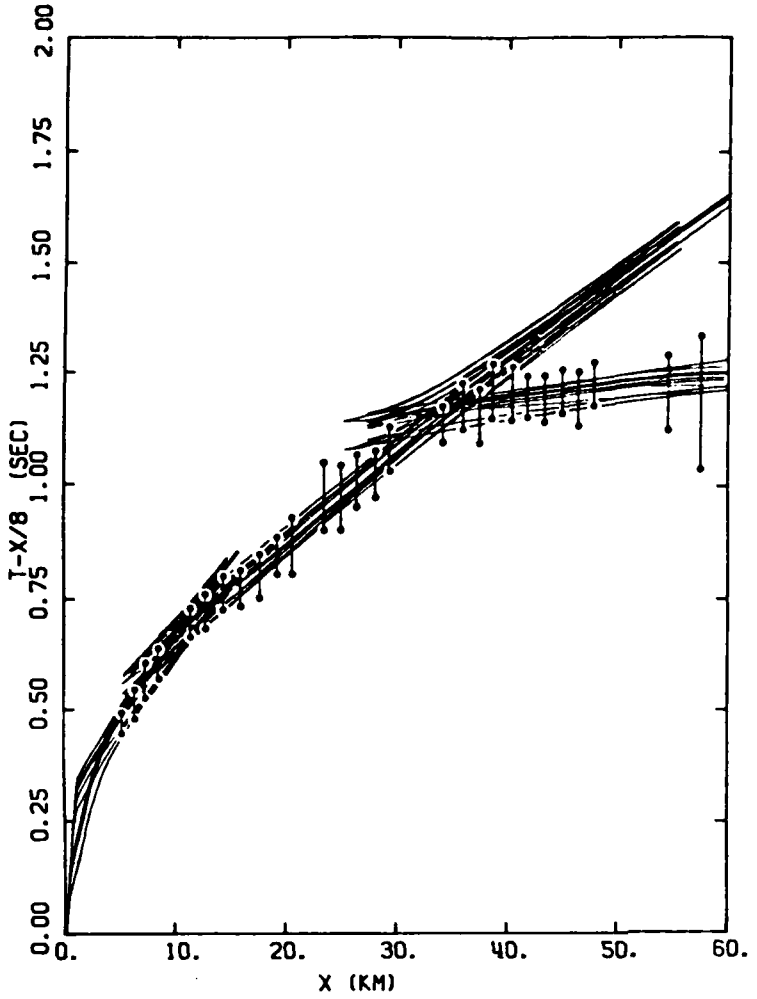


Figure 8(c)

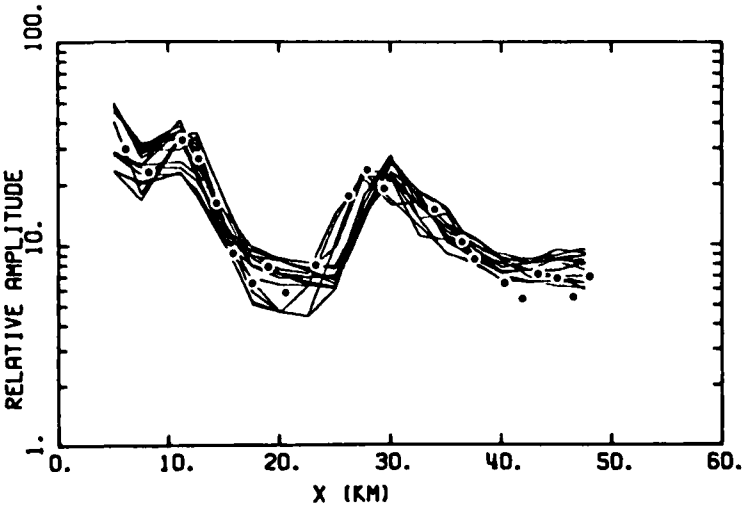


Figure 8(d)

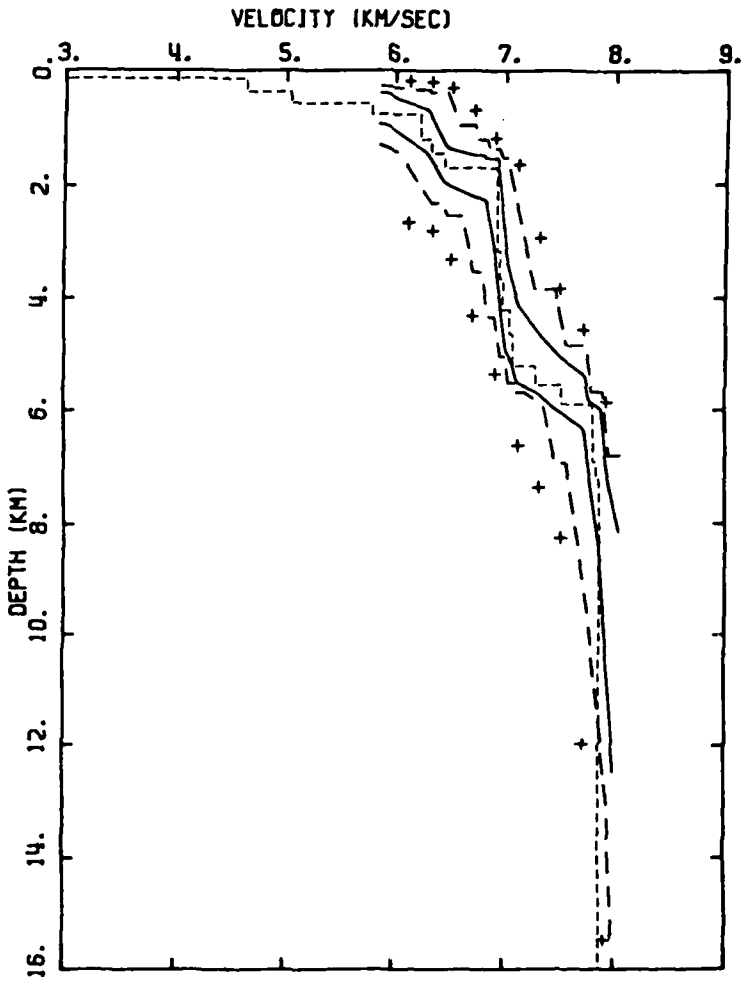


Figure 8(e)